Chaotic Mixing of Viscous Fluids by Periodic Changes in Geometry: Baffled Cavity Flow

Sadhan C. Jana, Mahari Tjahjadi, and J. M. Ottino
Dept. of Chemical Engineering, Robert R. McCormick School of Engineering and Applied Science, Northwestern University, Evanston, IL 60208

The baffled cavity flow—the first representative of a class of chaotic flows produced by time-dependent changes of geometries—is introduced and extensions to spatially-periodic systems proposed. Both experimental and computational results are reported. The goal of the study is to put into evidence some of the steps and considerations when designing a new mixing flow; a related objective is to demonstrate the use of an efficient and accurate numerical technique (BIEM) suitable for mixing studies in time-dependent geometries. Several parameters that affect the degree of mixing are studied: the mixing protocol—how the baffles are alternated and how many baffles are used in the flow during each piecewise motion; baffle sizes and shapes; geometrical and flow parameters, such as the wall displacement per period; and details of the baffle's motions.

Introduction and Setting: Modified Cavity Flows

Numerous experimental and computational studies have demonstrated the effectiveness of chaotic mixing in low Reynolds number flows, particularly in two-dimensional flows (for a recent review and background material, consult Ottino, 1990; Ottino et al., 1992). More recently, a handful of works have ventured into mixing experiments involving three-dimensional flows (Kusch and Ottino, 1992). Several prototypical systems have been extensively studied, and a few are thought of as well understood and have become emblematic of the general problem of chaotic mixing. Two such cases, both in two dimensions, are the eccentric cylinder flow (Chaiken et al., 1986; Swanson and Ottino, 1990) and the cavity flow (Chien et al., 1986; Leong and Ottino, 1989). These, as well as all two-dimensional systems studied to date, involve a fixed domain geometry with fluid motion generated by tangential motion of boundaries. Typically, chaos is introduced by time-periodic motion of two boundaries.

Figure 1a shows the streamline portrait of the simplest cavity flow, the lid-driven cavity flow. A motivation for this flow is that it resembles the cross-sectional flow of a single screw extruder (Middleman, 1977; Chella and Ottino, 1985). In this case, the motion is regular and there is no reorientation mechanism; stretching of fluid elements is linear with time and consequently mixing is poor. Figure 1b shows a plot of the circulation time of fluid particles, T, parameterized as a function of streamline position between the elliptic point and the wall. The mean value of the circulation time, $\langle T \rangle$,

$$\langle T \rangle = \int_0^1 T \, dy, \tag{1}$$

is 3.5 wall displacement units: that is, a typical particle on a streamline circulates once in every 3.5 units of top wall displacement. This is an important number to consider as many of the mixing results may be rationalized in terms of mean circulation time.

Mixing can be improved if two independent boundaries, say the top and bottom walls of the cavity, are moved independently (Leong and Ottino, 1989). However, it may be argued that the results obtained in terms of a two-wall moving cavity device cannot be readily adapted to practice and it might be important to think of other possibilities. What other alternatives are possible? One possibility is to introduce reorientation of fluid elements by periodically changing the geometry of the domain. A few possibilities, in the context of the lid-driven cavity flow, are suggested in Figure 2. In Figure 2a baffles placed at fixed location periodically enter and leave the flow domain, in Figure 2b baffles are attached to a time-

Present addresses of: S. C. Jana, The Benjamin Levich Institute, 1M Steinman Hall, City University of New York, New York; M. Tjahjadi, General Electric, Schenectady, NY.

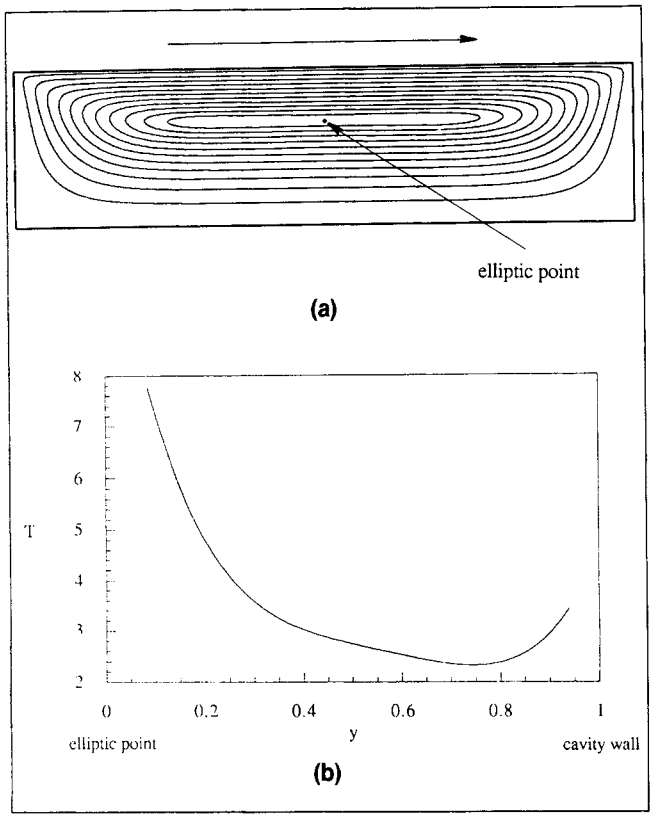

Figure 1. (a) Streamline portrait of standard cavity flow, $A = 4.0$, top wall moving; (b) circulation time $T = T(y, A)$, with y as the normalized distance from the central elliptic point, $A = 4.0$, top wall moving.

The total time taken by a fluid element to traverse a closed streamline is the circulation time; $T = 1$ corresponds to one cavity width top wall displacement, $D = 1$ (see Eq. 4).

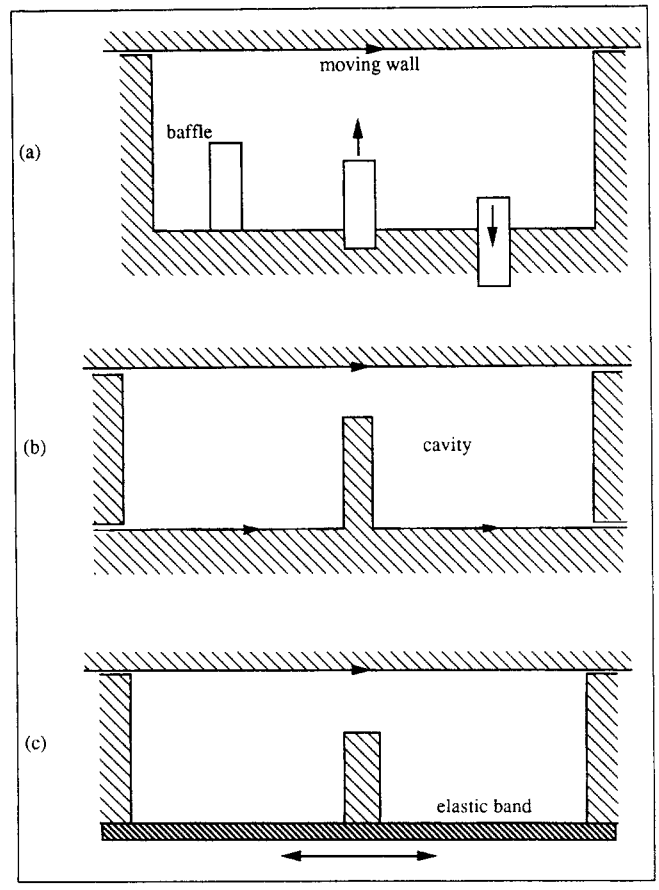

Figure 2. Possibilities of time-periodic baffled cavity flows: (a) push-pull mechanism; (b) baffle clamped to the bottom wall; (c) baffle clamped to an elastic band.

periodic moving wall, whereas in Figure 2c baffles are attached to an extensible wall. In the absence of leakage, all these examples involve flow singularities at the corners of the moving walls as well as corner eddies or Moffatt cells (Moffatt, 1964), see Figure 3. In Figure 2a, however, the corner eddies are short-lived as they are destroyed when the baffle is removed. In this work we will focus primarily on configuration 2a, but a few results are presented for 2b as well. The flow geometry is shown in Figure 3 along with the relevant parameters.

Figure 4 shows computer-simulated and experimental streamline portraits of baffled cavity flow with the baffles at three different locations (the experimental system will be described shortly). Alternate application of flows of Figures 4a(i–ii), following any of the prescriptions described in Figure 2, results in chaotic mixing. This can be rationalized as follows: A fluid element which just experienced exponential stretching in one baffle location now has the chance to experience another exponential stretching corresponding to a new baffle location. Alternatively, the streamlines of Figures 4b(i) and 4b(ii), when superposed on each other, show crossing and accordingly the flow is chaotic. Chaotic flows can be produced by combining Figure 4b(i–iii) in several ways, some of which are discussed later in the context of time-periodic flows.

The main objective of this study is to put into evidence some of the steps and considerations when designing a new—but by no means overly complex—mixing flow. A related objective is to demonstrate the use of an efficient numerical technique suitable for mixing studies involving time-dependent geometries. It is apparent that even within this rather idealized example there are several parameters that affect the degree of mixing: the so-called mixing protocol—how the baffles are alternated and how many baffles are used in the flow during each piecewise steady top wall motion; the baffle(s) size and

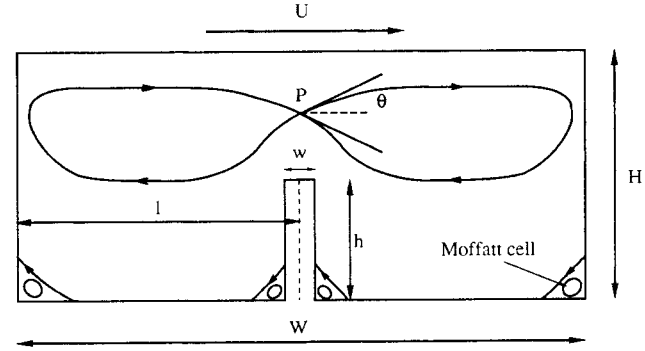

Figure 3. Flow geometry.

The hyperbolic point with coordinate (x_1^*, x_2^*) is denoted by P.

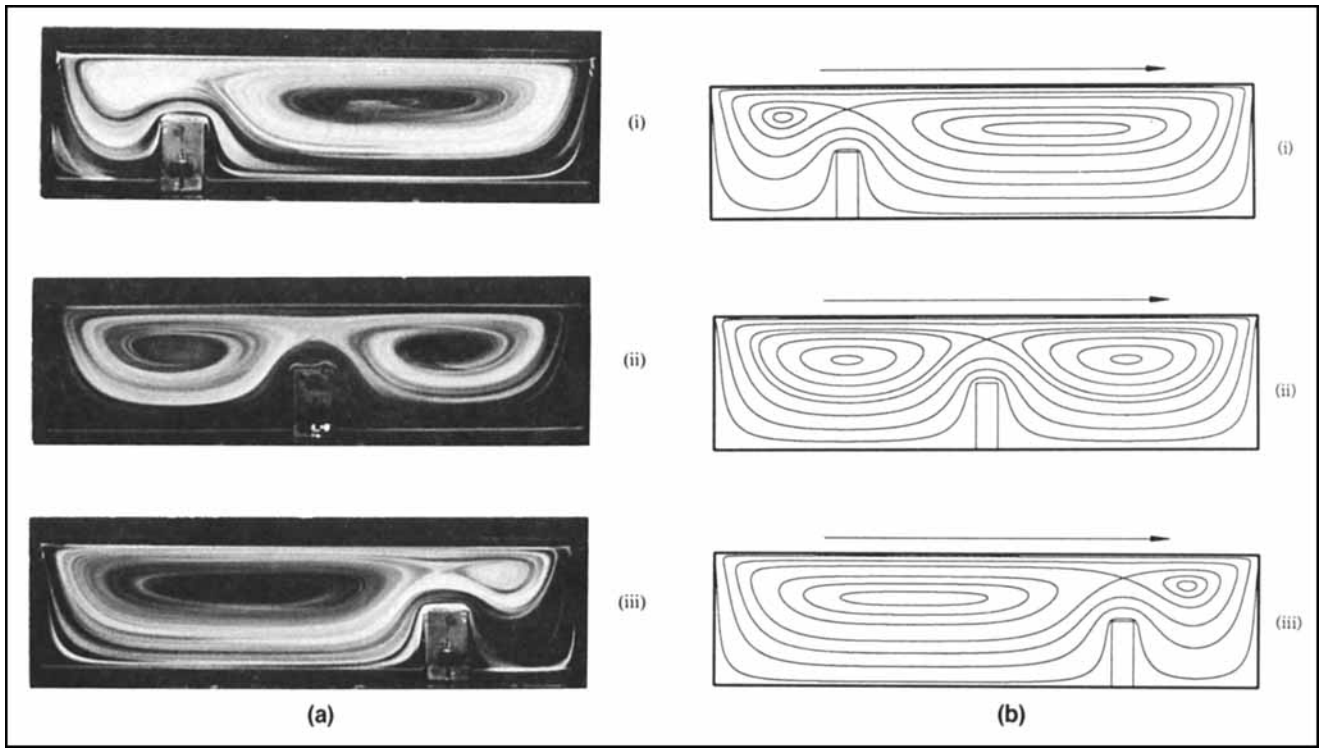

Figure 4. Streamline portraits of the baffled cavity flow, $A = 4.0$: (a) experimental; (b) computational.
(i) $l = 0.25W$, (ii) $l = 0.50W$, (iii) $l = 0.75W$.

shape; geometrical and flow parameters, such as wall displacement per period; and the specific details of the motion of the baffle themselves as described in Figure 2. Clearly, an exploration of all parameter space is neither desirable nor possible, and the question is how to proceed on the basis of incomplete information.

The first section of this article describes the flow geometry as well as the geometrical and flow parameters. The next sections focus on the experimental techniques and the computational aspects of flow solution, where boundary integral equation methods are reviewed briefly. The results and analysis form the bulk of the article with the focus being on steady and time-periodic flows and effects of protocols, along with alternative modes of operation.

The motion of the top wall implies that the flows studied here do not have simple symmetries (such as reflectional). Consequently, the chaotic flows themselves do not reveal symmetries as well, and it therefore follows that many of the conventional dynamical tools such as Poincaré maps and manifolds of periodic points, which depend heavily on symmetries, are not of much use in this study. As opposed to several past works produced by our laboratory the stress here is primarily on design aspects backed up by minimal usage of dynamical tools.

Flow Geometry and Parameters

Geometrical parameters

Figure 3 shows the schematic of the flow geometry. The aspect ratio of the cavity is defined by

$$A = W/H, \tag{2}$$

where W is the width and H is the height of the cavity. The baffle width is denoted by w and the height is parameterized by

$$b = h/H, \tag{3}$$

where h is the height of the baffle. Only rectangular baffles are used in this work. The width is fixed at $(1/20)W$. Baffles of nonrectangular geometry or baffles with rounded corners do not cause appreciable change in the qualitative nature of the flows and will not be considered here. The distance of the vertical axis of the baffle from the left static wall is given by l. In this work we use three values of l: $(1/4)W$, $(1/2)W$, and $(3/4)W$.

Flow parameters

As the fluid is highly viscous, the effect of inertia is neglected. The total displacement of the top wall in each piecewise steady motion is a measure of the energy input into the system and is defined as

$$D = \frac{UT}{W}, \tag{4}$$

where U is the top wall velocity and T is the time for one piecewise steady motion of the top wall with the baffle in place. The Strouhal number is defined as

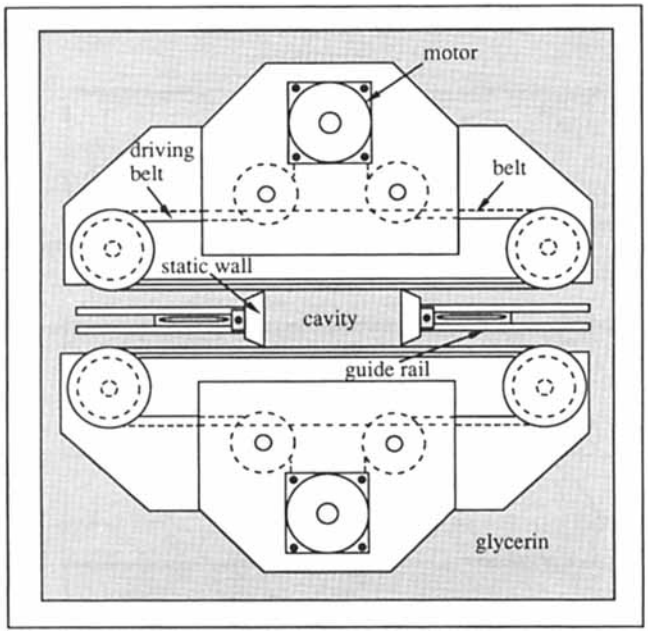

Figure 5. Experimental setup.

$$Sr = \frac{H^2/W}{UT} \tag{5}$$

and the Reynolds number is defined as

$$Re = \frac{(H^2/W)U}{\nu}, \tag{6}$$

where ν is the kinematic viscosity of the fluid. If the product of the Strouhal number and the Reynolds number is negligibly small, the fluid attains the wall velocity almost instantaneously and transient effects can be neglected.

Experimental Studies

The basic experimental apparatus used is the same as that used by Leong (1990), as shown in Figure 5. The aspect ratio of the cavity is maintained at 4.0 with $W = 0.254$ m and $H = 0.0635$ m. Baffles are either clamped to the bottom wall or inserted through selective ports on a bottom wall assembly (see Figure 2a). In the latter case, the bottom wall assembly replaces the bottom wall unit of Figure 5. The baffles and the bottom wall assembly are made of aluminum. The belt motion is produced by motors (Bodine NSH-11D5) controlled by computer using a Keithly System 570 Data Acquisition software. Motors are calibrated before experimental runs and belt speeds are accurate to 1%. The control schemes used in this work are similar to those used by Leong and Ottino (1989). The top wall always moves from left to right, and the bottom wall with baffle clamped on it moves either right to left or left to right with the direction and displacement controlled by the computer.

The fluid used is glycerin (Emery 916 Glycerin 99.7%) with a viscosity ~ 0.7 Pa·s and density 1.2×10^3 kg/m^3. The maximum belt speed used is 0.0085 m/s giving a maximum Reynolds number of 0.25. The Strouhal number ranges from 0.01–0.03. Fluid fills the entire apparatus, with the belt and part of its driving mechanism partially immersed in the fluid. Fluorescent dye (Cole-Parmer, type 295-15, 295-17) is used for flow visualization; the working fluid is glycerin. The dye is illuminated from above with UV lights (long range, Spectronix XX-40); blobs of dye are injected 0.005–0.01 m below the upper surface to obtain maximum illumination and to avoid free surface effects. The mixing patterns are photographed through the top with a Nikon N2000 camera, Nikkor micro f/4.0 105 mm lens, and Kodak Ektachrome 100 HC color slide film. The colored slides are then transferred into black-and-white film and printed on Kodak Polyfiber paper.

Flow Solution

Analytical solutions of the simple cavity flow and the baffled cavity flow are not available. Standard finite difference solution of the simple cavity flow has been used by many researchers in studies involving chaotic advection (Leong, 1990; Liu and Peskin, 1992). However, the solution of the baffled cavity flow using the finite difference method has some potential difficulties: (1) baffles of various shapes cannot be easily included; (2) a large computer memory is required for storage of the velocity field to model the time-changing geometry; and (3) much of the accuracy of the velocity field is sacrificed due to interpolation between the nodes. Boundary integral equation methods (BIEM), on the other hand, seem to be especially suited for this task. BIEM offers a combination of accuracy, flexibility to handle complex geometries, and computational efficiency. This method has been used in recent years in determining steady-flow patterns involving shear flows over ridges and cavities (Higdon, 1985, 1990), in periodically constricted channels (Pozrikidis, 1987) and flows through porous media (Larson and Higdon, 1986, 1987). Jana et al. (1993) have demonstrated the suitability of BIEM for studies on chaotic advection. A brief review of the technique follows. For more complete presentations, consult Higdon (1985) and Pozrikidis (1992).

The Stokes equations along with the equations of continuity form a set of elliptic partial differential equations which are amenable to solution by integral equation methods. In this work we formulate the problem in terms of the integral equations of first kind and express the velocity field in terms of the boundary velocities and the strength of unknown surface force distributions. The integral equations have the advantage of reduced dimensionality—two-dimensional flow can be studied in terms of line integrals. A set of linear algebraic equations results on discretization of the integral equations which are solved by LU decomposition to obtain the strength of the surface force. The velocity field at any interior point is then obtained analytically from these point forces without any need for interpolation.

Following Higdon (1985), the integral equations can be written as

$$u_i(x_0) = C \int_S [S_{ij}(x - x_0) f_j(x) - T_{ijk}(x - x_0) u_j(x) n_k] dS$$

$$i, j, k = 1, 2 \tag{7}$$

where u_i is the ith component of the velocity at a point x_0

inside the fluid, f_j is the jth component of the point force at a point x on the boundary, n is the normal at x pointing out of the fluid, and n_k is its kth component. S is the boundary of the fluid domain and

$$S_{ij}(\hat{x}) = \delta_{ij} \ln r - \frac{\hat{x}_i \hat{x}_j}{r^2} \tag{8}$$

is the free-space Green's function in two dimensions, where $\hat{x} = x - x_0$, $r = |\hat{x}|$, and T_{ijk} is the stress tensor associated with the Green's function. The factor C in Eq. 7 is $1/4\pi\mu$ when the point x_0 is inside the fluid and $1/2\pi\mu$ when the point x_0 is on the boundary of the domain.

As boundaries of the flow domain are straight, they are discretized using straight line elements, and the values of u and f are taken to be piecewise constant along each element and represented by their midelement values. To resolve the flows near corners we concentrate the boundary elements in that region. The discretized form of Eq. 7 is

$$u_i(x_m) = \sum_{n=1}^{N} A_{ij}(x_m, x_n) f_j(x_n) + \sum_{n=1}^{N} B_{ij}(x_m, x_n) u_j(x_n), \tag{9}$$

where x_m is a point in the flow and x_n is the discrete boundary point at the middle of element n. The expressions for A_{ij} and B_{ij} are

$$A_{ij}(x_m, x_n) = C \int_{-\delta_n/2}^{\delta_n/2} S_{ij}(x_m - x_n - \xi t_n) d\xi, \tag{10a}$$

$$B_{ij}(x_m, x_n) = -C \int_{-\delta_n/2}^{\delta_n/2} T_{ijk}(x_m - x_n - \xi t_n) n_k \, d\xi, \tag{10b}$$

where δ_n is the length of the nth boundary element, t and n are unit tangent and normal vectors to the nth element, and ξ is the local spatial variable. Estimates of the error due to discretization of the integral equation and piecewise smooth approximations of u and f along the elements are discussed in Higdon (1985) and Pozrikidis (1992).

The terms A_{ij} and B_{ij} are evaluated using ten-point Gauss-Legendre quadrature formula. Considering the point x_m on the boundary, the system of Eq. 9 is solved using LU decomposition to obtain the distribution of surface source f. Once f is obtained, the velocity in the interior of the fluid is calculated from Eq. 9 considering the point x_m inside the fluid.

Comparison of BIEM results with analytical solutions reveal that for single-particle tracking maximum tolerable error in the velocity field is 0.1%. The accurate computation of mixing patterns, on the other hand, is less stringent and can be achieved with error of about 1% (Souvatitis et al., 1994). All the computations presented here are deemed to be accurate within 1%. A few additional comments regarding issues of computational accuracy are presented in the final remarks.

Results and Analysis

Steady flows

Figure 4 shows the streamline portraits of the baffled cavity flow. Computational streamline portraits of Figure 4b are obtained by integrating equation

$$\frac{dx}{dt} = u(x); \quad \nabla \cdot u = 0, \tag{11}$$

where $x = (x_1, x_2)$, $u = (u_1, u_2)$ with suitably chosen initial conditions. In each case there is a hyperbolic critical point between the top wall and the baffle. Corner eddies are small and weak with circulation time $O(10^3\langle T\rangle)$ and may be ignored. Moreover, as baffles are periodically inserted and removed, corner eddies lose identity and their contents mix with the rest of the fluid.

The most salient feature of steady flows is the hyperbolic point P (see Figure 3). The local rate of stretching at a hyperbolic point varies with $e^{\lambda t}$, where $|\lambda_{1,2}| = \lambda$, subject to $\lambda_1 + \lambda_2 = 0$, and λ_1 and λ_2 are the real eigenvalues of the velocity gradient tensor, ∇u, evaluated at the hyperbolic point. The eigendirection corresponding to the positive eigenvalue determines the direction of stretching (θ), and the eigendirection corresponding to the negative eigenvalue is the direction of contraction (180°-θ) (see Figure 3). The values of λ and the direction of stretching and contraction calculated for three values of 1 are presented in Table 1 and for three values of b in Table 2.

The eigenvalues and the directions of stretching and contraction do not change appreciably as the baffle changes location between $0.25\,W \le 1 \le 0.75\,W$. Thus, a blob of dye placed on the hyperbolic point will stretch at nearly the same rate at these positions. The presence of a hyperbolic point is clearly beneficial. On the other hand, if the baffle is placed close to the static walls, then at a critical value of 1, a degenerate critical point with a cusp type of singularity appears in place of the hyperbolic point and one of the two elliptic points disappears. At the same time, the corner eddies grow up and occupy the entire narrow gap between the baffle and static wall. This is clearly an undesirable situation as this region will experience the least amount of motion. Computations reveal that this happens for $1 \le 0.1\,W$ and $1 \ge 0.9\,W$.

Table 1. Local Stretching Rate and Directions of Stretching at Hyperbolic Critical Point $P(=x_1^*, x_2^*)$ as a Function of Baffle Location (Figure 3)*

1	(x_1^*, x_2^*)	λ	θ
$0.25W$	$(1, 0.80H)$	4.92	17.7°
$0.5W$	$(1, 0.80H)$	5.06	18.3°
$0.75W$	$(1, 0.80H)$	4.92	17.7°

*Baffle height, $b = 0.5$.

Table 2. Local Stretching Rate and Directions of Stretching at Hyperbolic Critical Point $P(=x_1^*, x_2^*)$ as a Function of Baffle Height (Figure 3)*

b	(x_1^*, x_2^*)	λ	θ
0.25	$(0.5W, 0.710H)$	2.758	16.94°
0.5	$(0.5W, 0.8H)$	5.06	18.3°
0.75	$(0.5W, 0.790H)$	0.455	1.79°

*Baffle position, $1 = 0.5W$.

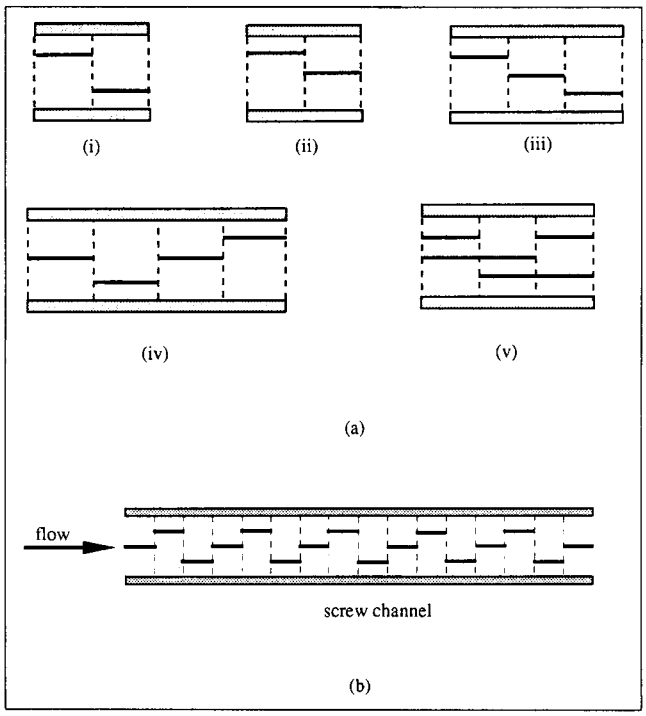

Figure 6. Motion of baffles and top wall: (a) protocols, (i) 13.., (ii) 12.., (iii) 123.., (iv) 2123.., (v) (12)(23)(31).., in (v) two baffles are in the flow at a time with (12) signifying baffles at 1 = 0.25 W and 0.50W are together in the flow; (b) typical view of baffle locations along the screw channel in a single-screw extruder using protocol 213..

Another design issue is the height of the baffle. The limit case $b=0$ corresponds to the standard cavity flow which is a poor mixing flow. The other limiting value is $b=1$, and this corresponds to two seemingly disconnected lid-driven cavity flows. Based on the values of Table 2, $b=0.5$ gives the largest local stretching rate and $b=0.75$ the least. From the analysis of steady flows, one might therefore argue that a value of $b=0.75$ is a bad choice for good mixing. This conclusion is, however, unwarranted, and indicates one of the pitfalls of basing conclusions on static information. In fact, in the next section when we study time-periodic flows, we find that $b=0.75$ produces better mixing than the other two cases because of the large deformation produced on material lines when baffles are inserted in the flow.

Time-periodic flows

Protocols. The protocol is a periodic sequence of motions describing the sequence by which baffles are put into the flow. Each protocol starts with a piecewise steady top wall motion with baffles in place. This is followed by switching the baffle position and repetition of top wall motion. The protocols used in this work are presented in Figure 6. If we designate the baffle locations at $1=(1/4)W$, $(1/2)W$, and $(3/4)W$ respectively as 1, 2, and 3, the protocol in Figure 6a(i) is denoted as 13. . . , 6a(ii) as 12. . . , 6a(iii) as 123. . . , 6a(iv) as 2123. . . , and 6a(v) as (12)(23)(31). . , the parenthesis indicating that two baffles are in the flow at a time. Numerous other protocols can be devised; however, we consider only the ones shown in Figure 6. Figure 6b shows a typical arrangement of baffles following protocol 213. . along the unwound screw channel of a single-screw extruder.

Deformation and stretching of material lines

As alluded to earlier, chaotic flows produce exponential stretching of material lines. This comes about by repeated stretching and folding; folding material lines stretch linearly and create more folds. This multiplicative process is repeated and consequently exponential stretching is produced. It should be noted that even under chaotic flow conditions the stretching is linear as long as there are no folds; exponential stretching begins at the onset of folding.

Numerical calculations. The numerical calculation of length stretch in a time-changing geometry flow is considerably more involved than in fixed geometry flows. The flow geometry changes continuously, when either a baffle is taken out of the flow and another is introduced simultaneously as in Figure 2a or when the baffle is displaced because it is physically attached to a moving wall as in Figures 2b or 2c. We model these processes by assuming M successive baffle configurations, that is, M successive instantaneous positions between its initial and final states and assign instantaneous baffle velocities to the boundary elements on it. We adopt quasi-steady approximations at each baffle configuration and assume that the fluid in contact attains the velocity of the baffle instantaneously. This is a reasonable approximation in our case as the fluid used is very viscous and experimental Strouhal number based on the time for changing the geometry is negligibly small.

For protocols with one baffle in the flow the distribution of surface force are determined $(M+1)$ times: once for fixed baffle location with the top wall in motion and M times for M baffle configurations with the top wall at rest. Similarly, for protocols involving two baffles at a time in the flow $(2M+1)$ evaluations are needed. The surface force distribution and boundary velocities for different baffle configurations are then stored in two-dimensional arrays. In this work we use 200 boundary elements and two values of $M=8$ and 16. For each baffle configuration, a fluid particle is advected for a time τ/M, where τ is the total time taken by the baffle to reach its final configuration. The major steps involved in the particle trajectory integration are outlined in Figure 7.

It is important to reiterate that in BIEM unknowns appear only at the boundaries. Therefore, the computer memory requirements to accommodate changes in geometry is much lower than the finite-difference or finite-element methods. In finite-difference or finite-element methods, the velocities at the nodal points for each baffle configuration must be stored.

Figure 8 shows instantaneous velocity fields corresponding to eight baffle configurations using protocol 13. . and the push-pull baffle mechanism of Figure 2a. The velocity field is rescaled to show only the salient features of the motion, such as the recirculating motion near the baffle roots; the length of the vectors do not correspond to the degree of motion. The instantaneous streamline portrait corresponding to Figure 8h is sketched in Figure 8i. Figure 9 shows a typical sequence of line deformation in three periods using protocol 13. . and eight configurations of upward and downward baffle motion; simulations with 16 configurations produce negligible change. The

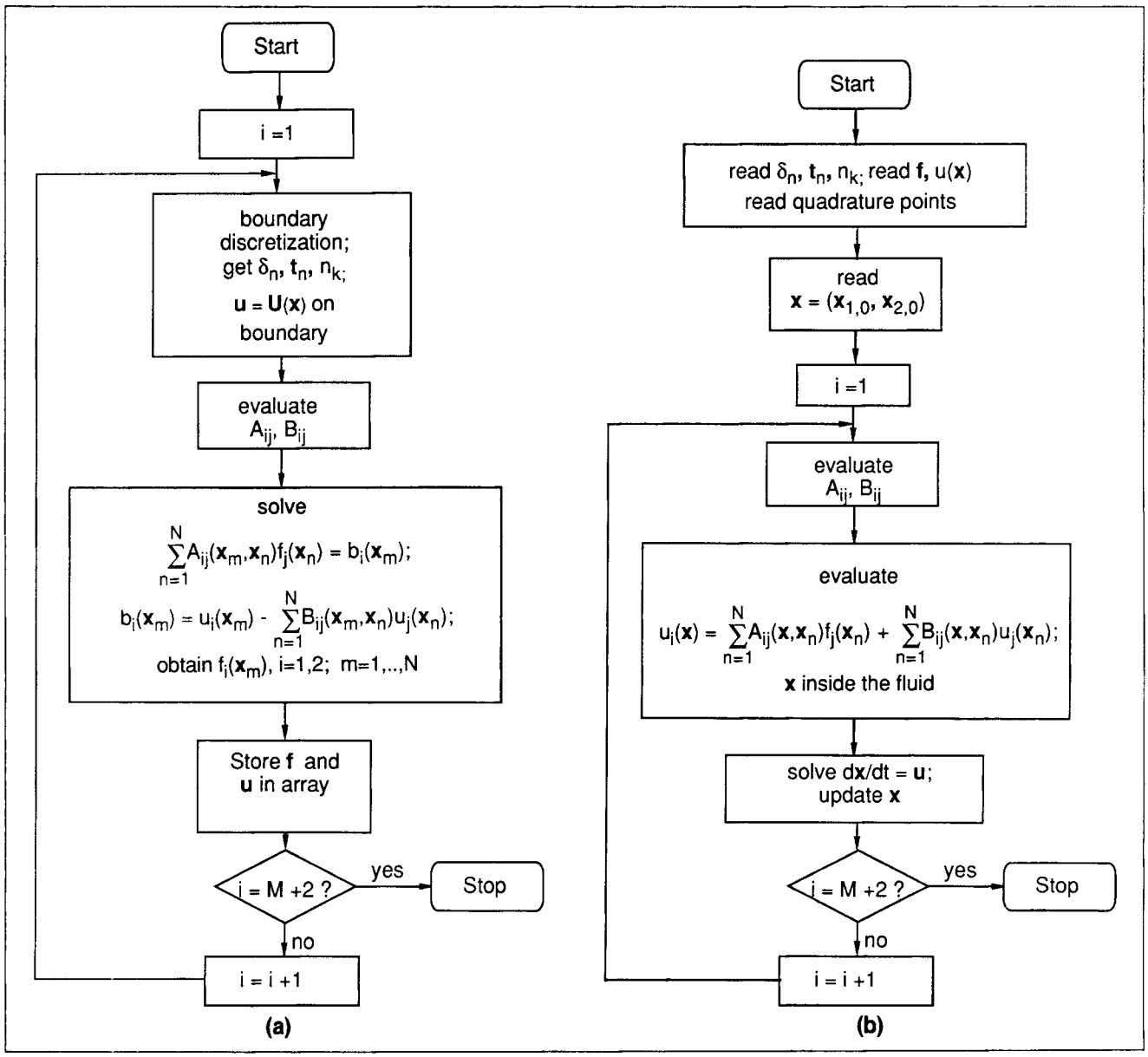

Figure 7. Algorithm for particle trajectory integrations in time-periodic baffled cavity flow with one baffle at a time in the flow and *M* baffle configurations: (a) solution of linear system of Eq. 9 for *f* and storage of data; (b) evaluation of interior point velocities and advection of a point for a period.

Values $i = 1$ and $M+2$ indicate top wall motion with fixed baffle.

deformation of the material line during baffle motion is also shown. The advection template develops in two periods of the flow (Figure 9f), on which finer scales are added in subsequent periods, as seen in Figure 9g. Also repeated stretching and folding produce exponential growth in the length of the material line.

Experiments. Figure 10 shows line deformation experiments using protocol 213 and the push-pull mechanism of baffles of Figure 2a. Photographs are chosen such that the baffle is always at position 2; this facilitates visual detection of the advection template or pattern, for example, similar patterns in Figures 10d–10f. Fine scales are added to the pattern as time progresses. The corners of the baffle with the bottom wall shows mixed dye structure. The eddies at the baffle corners of Figure 10b mix with the rest of the fluid due to shearing motion as a new baffle is inserted at position 1. However, the corners between the static walls and the bottom wall are devoid of any dye and are excluded from mixing because of corner eddies and invariant local flow patterns. Figure 10f also shows some regions of flow without any dye. If the experiment is run for long enough times, some of these regions may be filled with the dye leaving unfilled regions which we define as islands.

Figure 11a compares length stretch of a material line in several cavity flows computed numerically. A material line of equal length placed at identical location is advected using these flows. The length stretch in standard cavity flow and steady baffled cavity flow with the baffle fixed at the same location produce linear stretching. On the other hand, the time-periodic

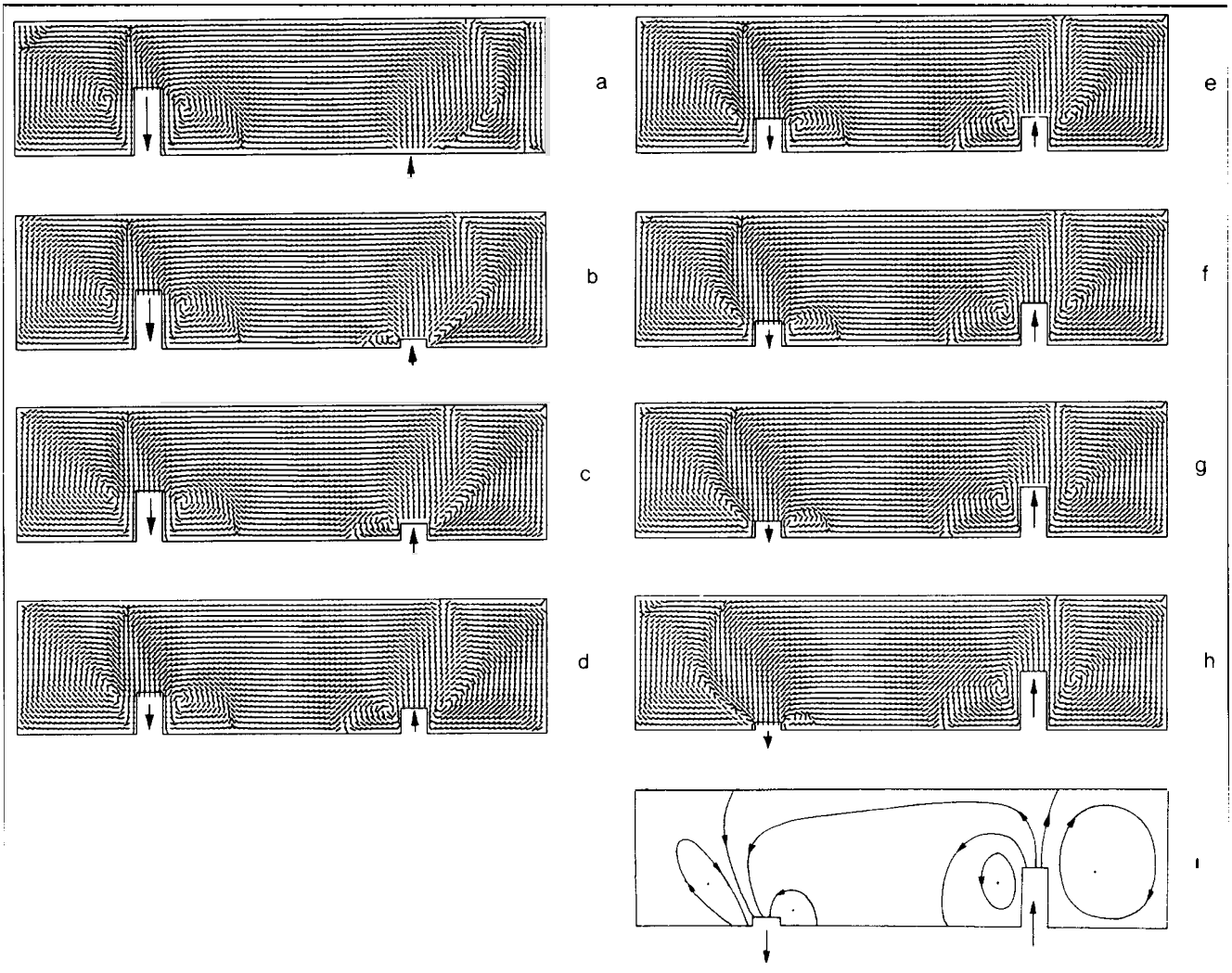

Figure 8. Eight instantaneous baffle configurations and corresponding velocity field in push-pull baffle mechanism, $A = 4.0$.

Baffles are at $l = 0.25W$ and $l = 0.75W$, respectively. (a-h) Instantaneous velocity field; (i) simplified sketch of the streamline portrait of (h). The velocities at each point is scaled by the speed at that point to capture the motion of the entire cavity.

baffled cavity flow produces exponential stretching as seen in Figure 10. A plot of the fractional dye area coverage in Figure 10 is presented in Figure 11b. Photographs of dye advection experiments are digitized in an image analyzer and a histogram of gray scales is prepared from it. The fraction of pixels that belong to the dye-covered area is then a measure of the fraction of the flow area covered by the dye, denoted as α, which in turn is a measure of the extent of mixing. The initial rate of increase in dye area is almost linear. As soon as the folds are created, the dye area increases exponentially. A plateau is reached after a certain number of periods when the dye area reaches a saturation value because of the boundedness of the flow (see Leong and Ottino, 1989).

Mixing patterns

The effects of protocols and geometrical parameters on mixing patterns are studied by observing the evolution of a blob or line of dye. In some cases, differences in goodness of mixing, as measured by the area coverage by the dye, are visually apparent as well. In other cases, however, where patterns appear to have almost equal area covered by the dye, we resort to fractional area coverage calculations using image analysis techniques to distinguish between them.

Effect of protocols. Protocols can have significant effects on mixing morphology as well as on the extent of mixing. In this work we measure the extent of mixing visually, by close visual examination of the dye advection patterns and quantitatively by image analysis. In visual inspection we differentiate mixing flows by comparing the apparent size of islands. This is often enough to discriminate among poor mixing flows. In good mixing flows, however, the islands are negligibly small in size and conclusions about the extent of mixing cannot be drawn only by visual inspection. Figure 12 shows the dye advection patterns obtained after 16 units of wall displacements using three different protocols. While it is readily apparent by visual inspection that protocol 13. . is less mixing than the other two, no conclusion can be drawn about protocol 213. . and 123. . But writing four repeating units together reveals that protocol 213. . and 123. . are identical in terms of the

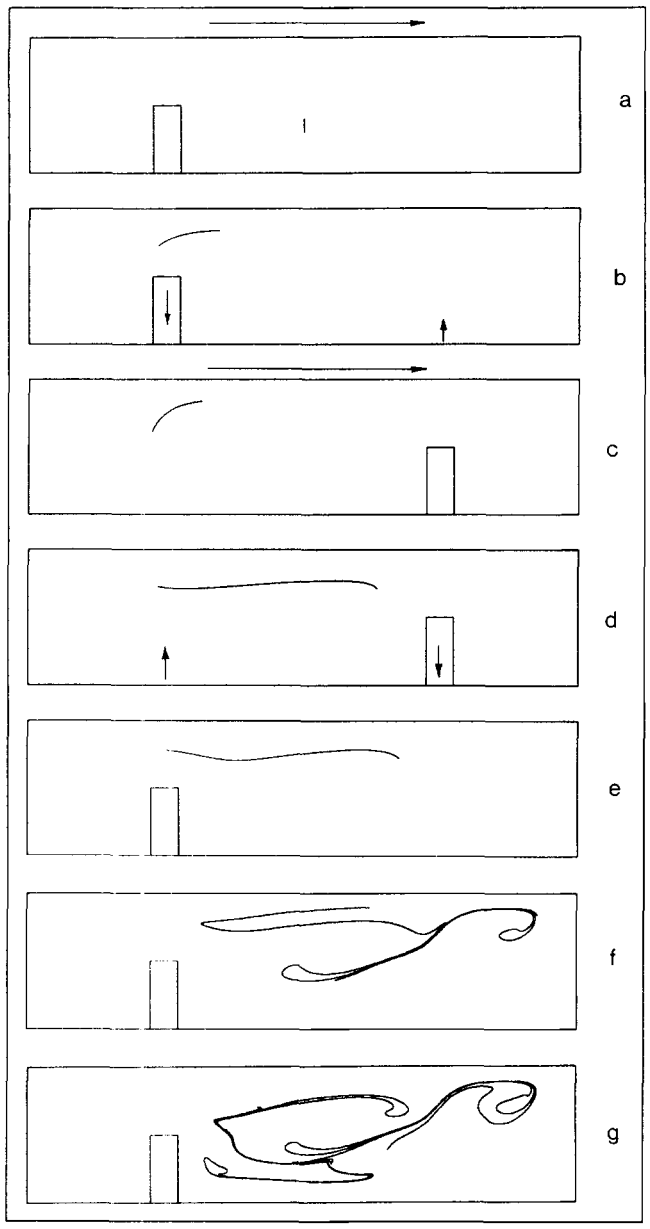

Figure 9. Computational line deformation in time-periodic baffled cavity flow using protocol 13.. and push-pull baffle mechanism, $A=4.0$, $M=8$, $D=1.0$.

(a) Initial line, baffle at $l=0.25W$; (b) $P=1D$; (c) baffle position switches, baffle at $l=0.75W$; (d) $P=2D$; (e) baffle position switches, baffle at $l=0.25W$; (a-e) describe one period; (f) deformed line after after two periods, $P=4D$; (g) deformed line after three periods, $P=6D$, P is the total unit of wall displacement.

switching of baffles: (213213213213. .) can be thought of as a sequence (321) which is the same as (123) in reverse order. So the extent of mixing must be the same in these protocols. However, the mixing patterns after a finite (small) time differ insofar as they depend on which baffle is switched on first. Image analysis of Figure 12 shows that protocols 123. . and 213. . with $\alpha=0.61$ are better mixing than protocol 13. . with $\alpha=0.56$.

Effect of b. As mentioned in the section on steady flows, the baffle height affects the local stretching rate at the hyperbolic critical point and the stretching rate goes down as the baffle approaches the top wall from the middle. In time-periodic flows, however, baffle height has different effects. Figure 13 shows experimental dye advection patterns obtained for three baffle heights after 16 units of wall displacements starting with almost identical initial line of dye. Inadvertently, identical lighting conditions were not used in taking the experimental photographs of Figure 13. Therefore, rather than using the same gray scale threshold value in image analysis, we use our best judgment to choose separate threshold values for each photograph and calculated the dye area coverage. It appears that the $b=0.25$ case is less mixing than the other two cases with best mixing achieved for $b=0.75$. Although the stretching rate at the hyperbolic point is low for the $b=0.75$ case, the larger extent of mixing is due to larger deformation produced on the dye streaks as the baffles are pushed in or pulled out. This, in fact, may be so as seen in the context of flow in a partitioned pipe mixer (Khakhar et al., 1987). However, the relevance of such a case to retrofitting applications in single-screw extruders is questionable and the case of $b=0.5$ might serve its purpose quite well.

Effect of D. The parameter D is the number of wall unit displacements during each top wall motion and measures the energy into the system. The value of $D=0$ means a flow generated only by baffle motions. On the other hand, $D\to\infty$ means steady baffled cavity flow. These two limiting cases produce poor mixing. Figure 14 shows the mixing structures produced by three values of D with the same protocol and taken after the same total number of wall-unit displacement. For a given number of total wall-unit displacement, flows with small D have a large number of baffle changes whereas flows with large D have a small number of baffle changes. For example, baffles are changed 28 times in Figure 14a, 14 times in Figure 14b, and 7 times in Figure 14c. Visual inspection can differentiate the extent of mixing in Figure 14; the best mixing is obtained at $D=1.0$.

Other modes of operation

The experimental advection patterns in Figures 10 and 12-14 are obtained with push-pull mechanism of the baffles, and in all cases only one baffle is used in the flow. Let us now investigate the effects of baffles moving with the bottom wall and effect of two baffles at one time in the flow.

Figure 15 shows the line deformation experiment of the moving baffle case with $D=1$. The baffle is clamped to the bottom wall, and after each top wall motion the baffle is carried to a new location by moving the bottom wall. The bottom wall movement also causes displacement to the fluid, which we take into account in calculating the total wall displacement. A close examination shows that the corners between the baffle and bottom wall do not have any dye in them—same set of eddies always stay at the corners and are, therefore, excluded from mixing. A visual comparison with Figure 10 shows that the moving baffle case is less mixing.

Figure 16 shows line deformation experiments with two baffles in place during the top wall motion. The corner eddies at the baffles are mixed in this case as well as in the one-baffle case in Figure 10. This flow is better mixing than in Figure 10 because of the larger number of deformation produced by the switching baffles as well as the presence of two hyperbolic points.

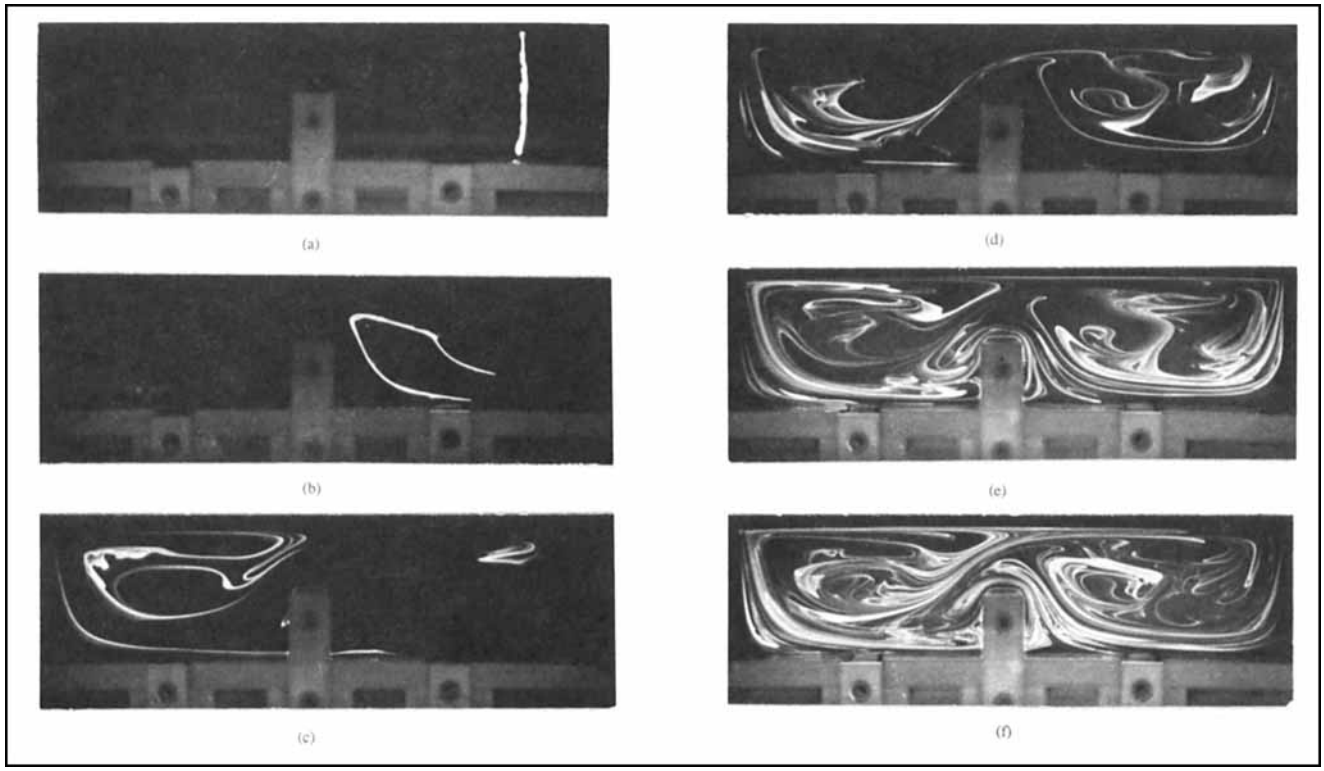

Figure 10. Experimental line deformation in time-periodic BCF using protocol 213.., $A = 4.0$, $D = 1.0$.

(a) Initial line; (b) $P = 1D$; (c) $P = 4D$; (d) $P = 7D$; (e) $P = 10D$; (f) $P = 13D$. P denotes the number of wall units of displacement.

In summary, the two-baffle case corresponding to the push-pull mechanism produces better mixing than the one-baffle case; moving baffle cases always exhibit unmixed regions at the root of the baffle and produce poor mixing; protocols 123. . and 213. . are better than protocol 13. . and, in fact, any protocol involving all three baffles produce good mixing; $D = 1$ cases are generally better than $D = 0.5$ and $D = 2.0$, implying that the circulation time corresponding to best mixing in a cavity partitioned into three subcavities is of order one; finally, of the three values of b tested, best mixing is achieved when $b = 0.75$.

Final Remarks

The purpose of this study was to put into evidence some of the considerations and steps necessary for the analysis of a new mixing flow. The fact that the flow is two-dimensional does not invalidate its engineering significance. In fact, it is hard to miss the relevance of these results to the retrofitting of existing mixing devices, such as single-screw extruders (Rauwendaal, 1986), and a few comments might be useful in this regard. A single-screw extruder consists of a screw rotating inside a close fitting cylindrical barrel; the fluid between the

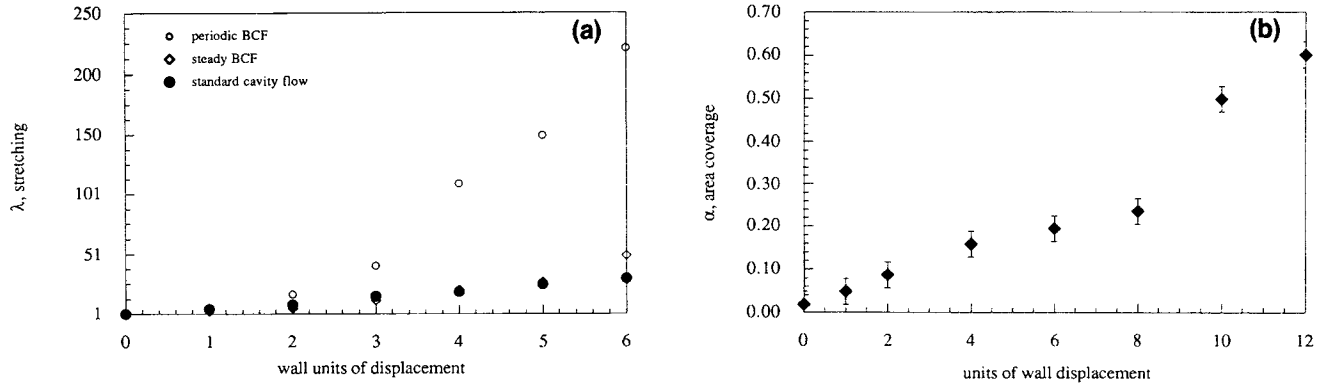

Figure 11. (a) Line stretching in several cavity flows, $A = 4.0$ (i) simple cavity flow, (ii) baffled cavity flow with the baffle at the middle, (iii) time-periodic flow with protocol 13..; (b) dye area coverage as a function of wall displacement of experimental advection patterns of Figure 10.

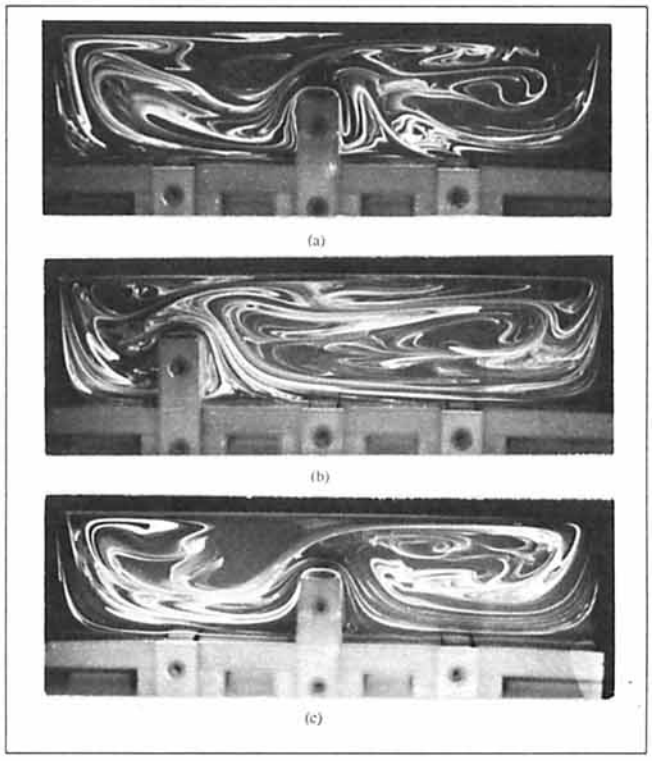

Figure 14. Effect of D on the extent of mixing, $A = 4.0$, 16 wall units of displacement in each case: (a) $D = 0.5$; (b) $D = 1.0$; (c) $D = 2.0$.

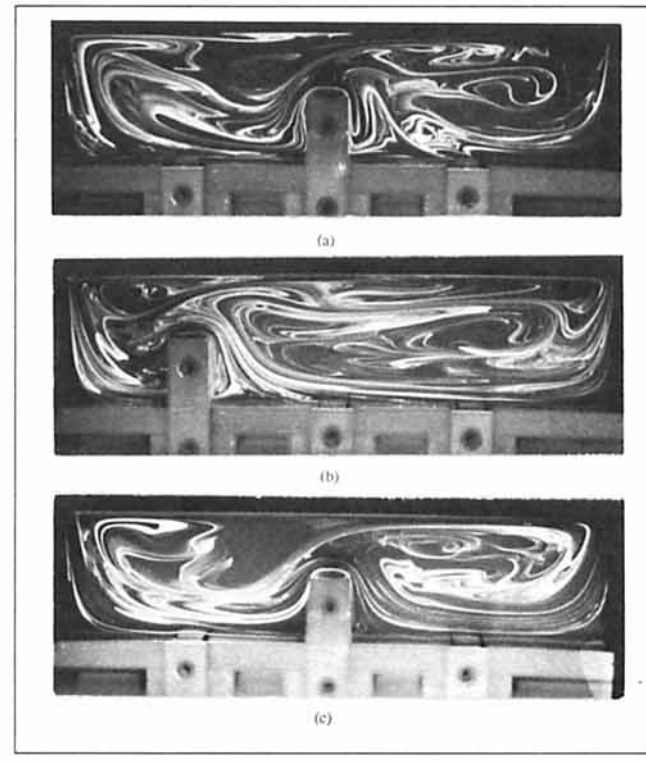

Figure 14. Effect of D on the extent of mixing, $A = 4.0$, 16 wall units of displacement in each case: (a) $D = 0.5$; (b) $D = 1.0$; (c) $D = 2.0$.

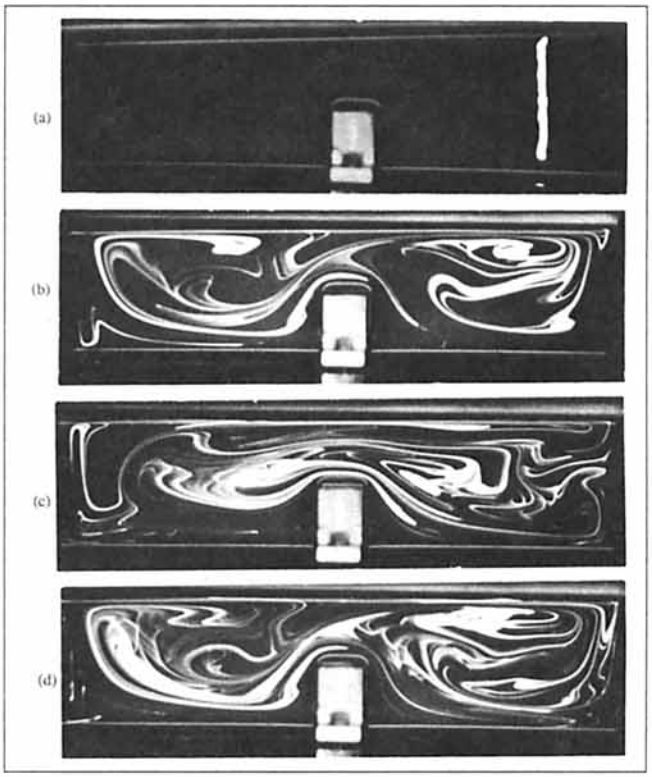

Figure 13. Effect of b on the extent of mixing, $A = 4.0$, 16 wall units of displacement in each case: (a) $b = 0.25$; (b) $b = 0.50$; (c) $b = 0.75$.

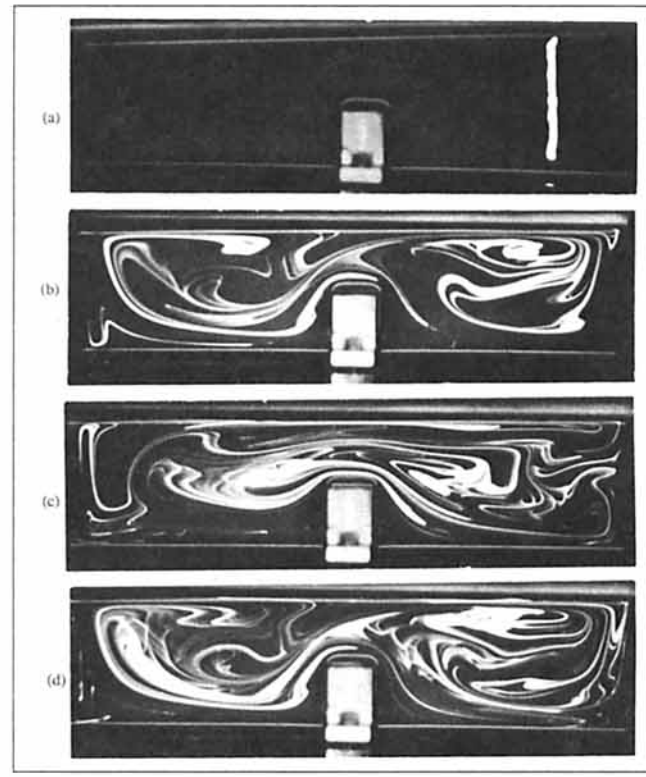

Figure 15. Line deformation experiments with moving baffles, $A = 4.0$, $D = 1.0$, protocol 213..: (a) initial line; (b) $P = 6D$; (c) $P = 10D$; (d) $P = 11D$. P is the total units of wall displacement.

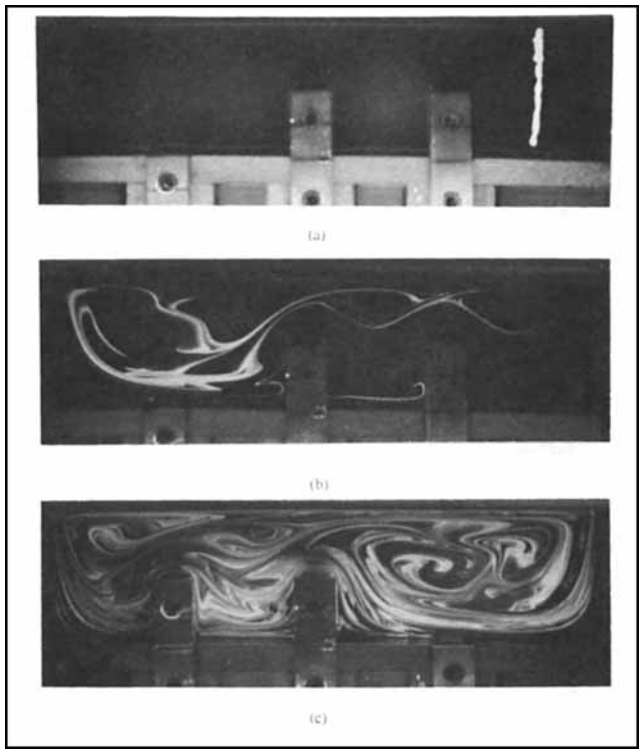

Figure 16. Line deformation experiments with two baffles in the flow using push-pull mechanism, $A = 4.0$, $D = 1.0$, protocol (32)(21)(13)..: (a) initial line; (b) $P = 4D$; (c) $P = 16D$. P is the total wall units of displacement.

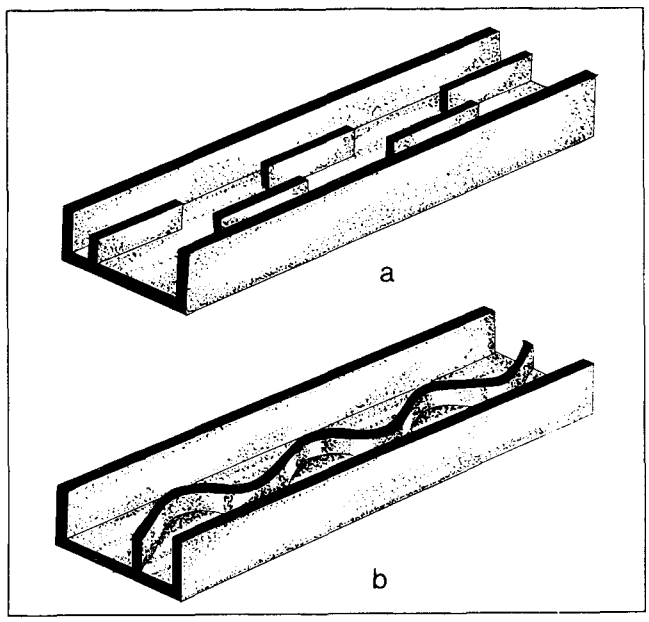

Figure 17. Possible ways of translating flow in a time-dependent geometry into a spatially dependent flow: (a) discontinuous baffles; (b) snake-like baffle.

threads of the screw is pushed forward due to the drag produced by the rotation of the screw. The relative motion of the screw and the barrel might be imagined as a plate or lid that moves diagonally on an unwound channel which can be decomposed into an axial flow, responsible for the pumping, and a cross flow corresponding to the lid-driven cavity flow (Figure 1).

As we have seen, the lid-driven cavity flow is a poor mixer but its baffled versions are not. It therefore follows that mixing in the single-screw extruder can be improved by somehow translating the time-periodic changes of geometry outlined in Figure 2 into a *spatially-periodic* change of geometry in the unwound channel representation. This concept is illustrated in Figure 17a and 17b. One possibility, inspired by Figures 2b and 2c, is to build a "snake-like baffle" within the primary extruder channel or, in the context of the actual screw, a helix of variable pitch. Another possibility, inspired by Figure 2a, is to introduce a discontinuous baffle as shown in Figure 17a. The case corresponding to Figure 17a has been reported before (Franjione and Ottino, 1992) and it goes back to studies by Leong (1988). Closer inspection reveals that both correspondences are only approximate (for example, baffles do not go in and out in Figure 17a; there are no corner singularities in Figure 17b as opposed to Figure 2b). Nevertheless, it is safe to expect that cross-sectional mixing can be greatly improved in both cases. The length stretch in the channel without the baffles is linear and mixing is poor (Franjione and Ottino, 1991). However, the case corresponding to Figure 17a is expected to produce better mixing than Figure 17b as the corner eddies would persist as tubes at the root of the baffle in Figure 17b and would not mix with the rest of the fluid. Another factor, to be taken into account when analyzing three-dimensional mixing in the actual extruder, is that the axial and cross flows are coupled. Although this would make the solution of flows more involved, the analysis presented in this work can be readily adapted to such a case.

Let us now turn to issues that have to do with the chaotic nature of the flow itself. The fact that a flow is chaotic impinges on what can be computed, for how long, and how accurately. During the past few years, there has been a considerable improvement in the understanding of all these issues (Souvaliotis et al., 1994); in light of the widespread use of flow simulation packages, a few comments would appear to be especially pertinent. The most stringent computational test corresponds to tracking of an individual trajectory. A small degree of error in the velocity field, $O(0.1\%)$, can produce large deviation in the computed trajectory or pathlines after just two or three circulation times. This does not mean, however, that meaningful computations are impossible. In fact, if this were taken literally to the extent that an experiment can never be exactly duplicated, experiments would be irreproducible. (It is manifestly impossible to place a blob of dye in the same location twice.) What matters is what gets computed. Thus, if the objective is to know what happens to a blob of material, as in Figure 10, the conditions are less stringent, and a $O(1\%)$ error in the velocity field is in fact acceptable insofar as the large-scale mixing structure is concerned (such as capturing folds, and large and small islands). This is so due to the shadowing lemma (Grebogi et al., 1990).

In simple terms, what this lemma states is that associated with almost every initial condition in the error-free dynamical system, there is a nearby initial condition in the simulated

systems that stays close ("shadows") to the actual trajectory for long times. Computing a single error-free trajectory is hard, but computing lots of trajectories at once produces an accurate picture of the system at large. Next in line come root-mean-square deviations in the velocity field of about 2-3%. Such deviations in the velocity field, with respect to some reference case, can be, for example, produced by rheological differences over a Newtonian case, temperature variations over an isothermal reference, and so on. Deviations by rheological differences occur, for example, in the flow of shear thinning or elastic fluids and clearly show the importance of these effects (Niederkorn, 1993; Niederkorn and Ottino, 1993). In this case, substantial and consistent variations in large-scale patterns are seen; for example, a large island present in the viscoelastic case might not be present in the Newtonian case. These are the issues that should be considered when designing a new mixing system.

Acknowledgment

This research was supported by the Department of Energy, Division of Basic Energy Sciences, monitored by Dr. Oscar Manley.

Notation

$\langle T \rangle$ = mean circulation time, Eq. 1
A = aspect ratio, Eq. 2
A_{ij}, B_{ij} = coefficients, Eqs. 9 and 10
b = dimensionless baffle height, Eq. 3
C = constant, Eq. 7
D = displacement of moving walls, measured in cavity width units, Eq. 4
f_j = jth component of the surface force, Eqs. 7 and 9
h = baffle height, Figure 3
H = cavity height, Figure 3
l = distance between the baffle axis and the left static wall, Figure 3
M = number of baffle configurations
n_k = kth component of the unit normal vector, Eqs. 7 and 10b
Re = Reynolds number, Eq. 6
Sr = Strouhal number, Eq. 5
t_n = unit tangent vector on nth boundary element, Eq. 10
T = time for piecewise steady motion of cavity wall, Eqs. 4 and 5
$T(y)$ = circulation time, Eq. 1
u_i = ith component of velocity, Eq. 7
U = velocity of moving cavity wall
W = cavity width, Figure 3
x = position of a fluid particle, Eq. 11
x_1^*, x_2^* = coordinates of the hyperbolic point P, Figure 3, Tables 1 and 2
x_m, x_n = middle point of the m and nth boundary elements, respectively
y = normalized vertical coordinate from the elliptic point, Figure 1

Greek letters

α = fractional dye area coverage, Figure 11b
δ_{ij} = Kronecker delta function
δ_n = length of the nth boundary element, Eq. 10a
λ = length stretch, Figure 11a
λ_1, λ_2 = eigenvalues of the velocity gradient tensor
ν = kinematic viscosity
ξ = local length variable on boundary element, Eq. 10

Literature Cited

Chaiken, J., R. Chevray, M. Tabor, and Q. M. Tan, "Experimental Study of Lagrangian Turbulence in a Stokes Flow," *Proc. Roy. Soc. Lond.*, **A408**, 165 (1986).
Chella, R., and J. M. Ottino, "Fluid Mechanics of Mixing in a Single-Screw Extruder," *Ind. Eng. Chem. Fundam.*, **24**, 170 (1985).
Chien, W.-L., H. Rising, and J. M. Ottino, "Laminar Mixing and Chaotic Mixing in Several Cavity Flows," *J. Fluid Mech.*, **170**, 355 (1986).
Franjione, J. G., and J. M. Ottino, "Symmetry Concepts for the Geometric Analysis of Mixing Flows," *Phil. Trans. Roy. Soc.*, **338**, 301 (1992).
Grebogi, C., S. M. Hammel, J. A. Yorke, and T. Sauer, "Shadowing of Physical Trajectories in Chaotic Dynamics: Containment and Refinement," *Phys. Rev. Lett.*, **65**, 1527 (1990).
Higdon, J. J. L., "Effect of Pressure Gradients on Stokes Flows over Cavities," *Phys. Fluids A*, **2**, 112 (1990).
Higdon, J. J. L., "Stokes Flow in Arbitrary Two-Dimensional Domains: Shear Flow over Ridges and Cavities," *J. Fluid Mech.*, **159**, 195 (1985).
Kusch, H. A., and J. M. Ottino, "Experiments on Mixing in Continuous Flows," *J. Fluid Mech.*, **236**, 319 (1992).
Larson, R. E., and J. J. L. Higdon, "Microscopic Flow Near Surface of Two-Dimensional Porous Media: 1. Axial Flow," *J. Fluid Mech.*, **166**, 449 (1986).
Larson, R. E., and J. J. L. Higdon, "Microscopic Flow Near Surface of Two-Dimensional Porous Media: 2. Transverse Flow," *J. Fluid Mech.*, **178**, 119 (1987).
Leong, C. W., Univ. of Massachusetts, unpublished (1988).
Leong, C. W., "Chaotic Mixing of Viscous Fluids in Time-Periodic Cavity Flows," PhD Thesis, Univ. of Massachusetts, Amherst (1990).
Leong, C. W., and J. M. Ottino, "Experiments on Mixing Due to Chaotic Advection in a Cavity," *J. Fluid Mech.*, **209**, 463 (1989).
Liu, M., and R. L. Peskin, "Chaotic Dynamics of Finite Particles in 2-D Periodic Cavity Flows," *Bull. Am. Phys. Soc.*, **37**, 1735 (1992).
Middleman, S., *Fundamentals of Polymer Processing*, McGraw-Hill, New York (1977).
Moffatt, H. K., "Viscous and Resistive Eddies Near a Sharp Corner," *J. Fluid Mech.*, **18**, 1 (1964).
Niederkorn, T. C., "Chaotic Mixing of Non-Newtonian Fluids in Time-Periodic Flow," PhD Diss., Northwestern Univ. (1993).
Niederkorn, T. C., and J. M. Ottino, "Mixing of Viscoelastic Fluids in Time-Periodic Flows," *J. Fluid Mech.*, **256**, 243 (1993).
Ottino, J. M., F. J. Muzzio, M. Tjahjadi, J. G. Franjione, S. C. Jana, and H. A. Kusch, "Chaos, Symmetry, and Self-Similarity: Exploiting Order and Disorder in Mixing Processes," *Sci.*, **257**, 754 (1992).
Ottino, J. M., *The Kinematics of Mixing: Stretching, Chaos, and Transport*, Cambridge University Press, Cambridge, reprint (1990).
Pozrikidis, C., *Boundary Integral and Singularity Methods for Linearized Viscous Flow*, Cambridge University Press, Cambridge (1992).
Pozrikidis, C., "Creeping Flow in Two-Dimensional Channels," *J. Fluid Mech.*, **180**, 495 (1987).
Rauwendaal, C., *Polymer Extrusion*, Carl Hanser Verlag, Munich (1986).
Souvaliotis, A., S. C. Jana, and J. M. Ottino, "Potentialities and Limitations of Computer Simulations," *AIChE J.*, accepted (1994).
Swanson, P. D., and J. M. Ottino, "A Comparative Computational and Experimental Study of Chaotic Mixing of Viscous Fluids," *J. Fluid Mech.*, **213**, 227 (1990).

Manuscript received July 16, 1993, and revision received Dec. 10, 1993.